

Article

Analysis of LC-LC² Compensated Inductive Power Transfer for High Efficiency and Load Independent Voltage Gain

Md Morshed Alam ^{1,*} , Saad Mekhilef ^{1,2} , Hussain Bassi ³ and Muhyaddin Jamal Hosin Rawa ⁴

¹ Power Electronics and Renewable Energy Research Laboratory, Department of Electrical Engineering, University of Malaya, 50603 Kuala Lumpur, Malaysia; saad@um.edu.my

² Center of Excellence in Renewable Energy and Smart Grid, King Abdulaziz University, Jeddah 21589, Saudi Arabia

³ Department of Electrical and Computer Engineering, King Abdulaziz University, Rabigh 21911, Saudi Arabia; hmbassi@kau.edu.sa

⁴ Department of Electrical and Computer Engineering, King Abdulaziz University, Jeddah 21589, Saudi Arabia; mrawa@kau.edu.sa

* Correspondence: malameee0602059@gmail.com

Received: 30 June 2018; Accepted: 27 August 2018; Published: 24 October 2018



Abstract: A novel LC-LC² compensated resonant converter topology with high efficiency and good controllable voltage gain is presented in this paper. An additional receiving side inductor working together with the receiving coil has the contribution to work with a large range of air gap distance. Due to this property, proposed compensation technique is effective for IPT based EV charging application. Voltage gain with independent of load and input impedance having ZPA of the proposed resonant converter are observed by the frequency domain analysis. On the other hand, time domain analysis gives the circuit operation. A 500 W LC-LC² compensated resonant converter prototype is built to testify the theoretical analysis. To observe the efficiency-comparison, an S-SP compensated resonant converter with a similar amount of output power under different air gap is also presented. In order to justify the effectiveness, the proposed compensation method is verified by the laboratory results. The highest efficiency of the proposed compensated resonant converter is 93% with output power of 500 W at 140-mm air gap between the two sides of the IPT (inductive power transfer) transformer.

Keywords: load independent voltage gain; zero phase angle (ZPA); resonant converter; inductive power transfer (IPT)

1. Introduction

Technology of inductive power transfer (IPT) delivers power to the utility load via magnetic coupling, is more suitable and versatile energy transfer method in comparison with traditional methods. Due to the low maintenance cost and highly reliable operation, IPT system is more popular for a large area of applications including battery charging of electric vehicles [1–4], home appliances [5], biomedical treatments [6,7] and other areas associated with industries [8]. IPT technology normally handles a large variation of loading and magnetic coupling coefficient. In order to achieve maximum efficiency and enhanced controllable output, researcher's works have been observed on the basis of wide variation of IPT parameters [3,9–18].

The ruling parameters that affect the efficiency and controllability of output power are: coupling factor and misalignment tolerance. In order to obtain high coupling factor and misalignment tolerance, most of the researchers have focused on the optimization of IPT-parameters [9,19,20]. Another key

factor that affects the efficiency and output power controllability of IPT system is the compensation network. Various types of compensation networks by the aid of control technique have been presented and explained in details [16–18,21–27]. Four conventional compensation techniques that are widely used named as S-S (series-series), S-P (series-parallel), P-S (parallel-series), and P-P (parallel-parallel). Among four compensation techniques, P-S and P-P compensated IPT systems are free from danger for the source if the pick-up coil is not present. But these compensation techniques are not suitable to transfer the rated power in case of misalignment condition, as resonant capacitor value strongly depends on the magnetic coupling coefficient and the output load [12]. Consequently, S-S and S-P topologies are widely used in many applications like [10,11,25]. The efficiency of the S-S compensated converter is high when self-inductances of the transmitter and receiver are tuned [10]. Comparison between self-inductance compensation and leakage inductance compensation of S-S topology is presented in [7,25]. However, self-inductance tuned by the S-S compensation presents output voltage which is very sensitive to the output load changes [10]. In order to improve the sensitivity of the output voltage under wide load variation, S-S compensated converter is designed to operate around the frequency of load independent voltage gain [7,25]. On the other hand, input impedance having ZPA is not maintained at a frequency of voltage gain where load is independent. Therefore, efficiency may be lower because of circulating current. In [10], a tradeoff between output voltage controllability and efficiency of the S-S topology is presented. Moreover, the problem still exists as tuning of compensating capacitors is not easy to obtain. Since, S-P compensation provides input impedance with ZPA at a frequency of load independent voltage gain [16]; this technique is suitable for high power applications like [26]. Furthermore, S-P compensation is not effective for a wide range of coupling coefficient and misalignment as load independent voltage gain is inversely related to the coupling coefficient [18]. To maintain a unique output power under the changes of coupling, SP-S compensation network was presented in [17]. There is a large number of research works based on LCL compensation [13–15,28]. In [28], a series-parallel LCL tuned unity pick up was presented, that provides uninterrupted power though it reflects reactive power to the source [29]. Another compensation topology with high efficiency named LCC was used in the areas of EV (electric vehicle) charging [23,27]. Here, load independent voltage gain under coupling changes is very much difficult to obtain because of self-coupling between the compensation inductor and main coil. At a frequency of load independent voltage gain, input impedance with ZPA and high power transfer efficiency can be obtained in S-SP compensated resonant converter [18]. Higher-order harmonics are the main limitation of this compensation technique, injected into the rectifier network. These higher order harmonics create the problems for filter design.

A novel LC-LC² compensation network for IPT system is proposed in this paper which provides input impedance with ZPA and high efficiency at a frequency of load independent voltage gain like S-SP compensated resonant converter. Here, an additional receiving side inductor working parallel to the magnetizing inductance has the great contribution to work under a large range of air gap distance. Because, the parallel effect of additional inductor and magnetizing inductance minimizes the air gap variation effect.

This paper is presented as like: Proposed LC-LC² compensation is introduced by Section 2. Section 3 provides the frequency domain analysis of the proposed LC-LC² compensation based resonant converter. Section 4 presents time domain analysis of the proposed LC-LC² compensation based resonant converter. Section 5 represents the analysis of the experimental results. Finally, Section 6 is summarized.

2. Proposed LC-LC² Compensation

Analysis of input impedance with ZPA and voltage gain at a frequency where load is independent is described in this section. In this case, T-model for IPT transformer having turn ratio 1: n is chosen. In the T-model, L_{l1} and L_{l2} depict the leakage inductances of the transmitter and receiver coil of IPT transformer respectively whereas L_M is the magnetizing inductance. In case of S-SP compensated resonant converter, Ref. [18] capacitor C_{f2} for compensating L_M is introduced to the S-S compensated resonant converter. Although input impedance with ZPA and voltage gain with load independent are obtained, higher order harmonics are injected to the rectifier network. To minimize the air gap

variation effect as well as the effect of higher order harmonics, an inductor L_{f2} parallel with L_M is launched to the S-SP compensated resonant converter. In this case, the equivalent parallel inductance of n^2L_M and L_{f2} are compensated by C_{f2} . This equivalent inductance is expressed as,

$$L_{Mf} = n^2L_M \parallel L_{f2} = \frac{n^2L_M L_{f2}}{n^2L_M + L_{f2}} \tag{1}$$

For a resonant frequency, a variation of the air gap (i.e., mutual inductance changes) does not affect the load independent voltage gain and the efficiency so much, because of the parallel effect of L_{f2} with L_M . This is observed in Figures 6 and 8.

The equivalent circuit of the LC-LC² compensation network by the help of T-model is depicted in Figure 1. If above equivalent inductance as well as all leakage inductances of the proposed IPT transformer are compensated at a time,

$$\omega_r = \frac{1}{\sqrt{L_{l1}C_1}} = \frac{1}{\sqrt{L_{l2}C_2}} = \frac{1}{\sqrt{L_{Mf}C_{f2}}} \tag{2}$$

where the resonant frequency is ω_r . L_{l1} , L_{l2} and L_{Mf} are compensated by C_1 , C_2 and C_{f2} respectively. It can be observed that at the resonant frequency, the output voltage gain of this resonant converter is independent of load and coupling coefficient changes. Also, ZPA of the input impedance is maintained under the full compensation condition.

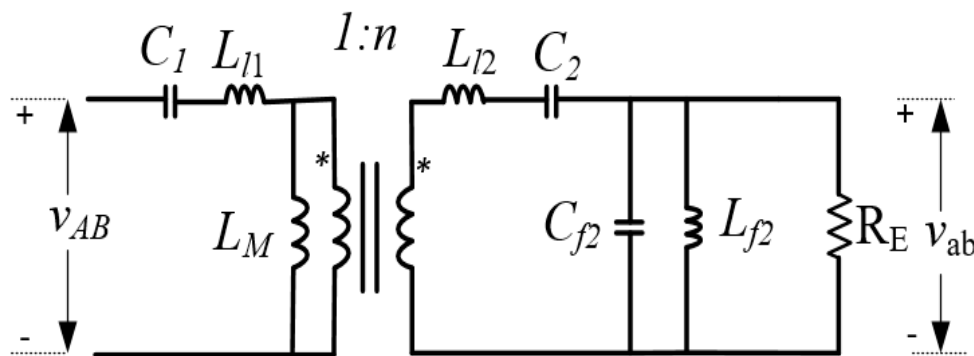


Figure 1. Equivalent circuit of the LC-LC² compensation network.

3. LC-LC² Compensated Resonant Converter Using Frequency Domain Analysis

In this section, voltage gain with load independence as well as input impedance with ZPA of the proposed LC-LC² compensated resonant converter have been explained in brief. The proposed LC-LC² compensated resonant converter is shown in Figure 2.

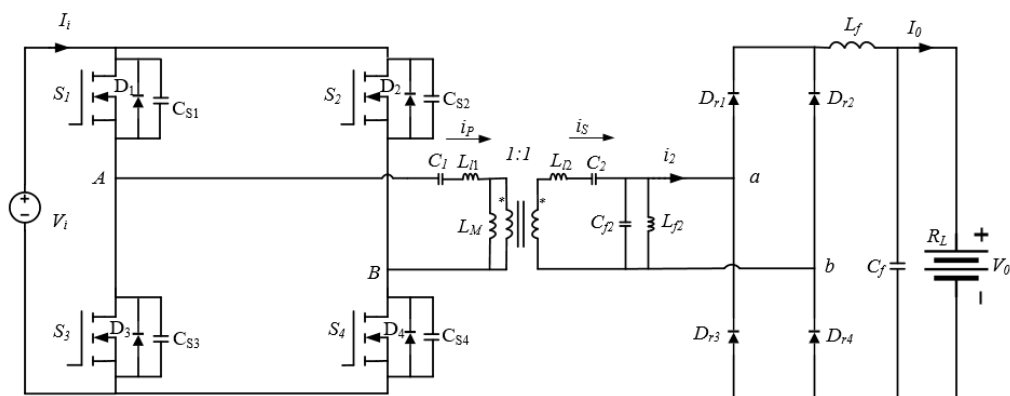


Figure 2. Proposed LC-LC² compensated resonant converter.

Here, high frequency inverter is operated by the input dc supply of V_i whereas, V_0 is the voltage across the battery having resistance R_L . L_f and C_f are used for filtering purpose in order to get pure dc after the high frequency rectifier.

By the help of Kirchoff's voltage law, fundamental components of V_{LM} , V_{AB} and V_{ab} can be expressed as,

$$V_{LM} = V_{AB} \frac{j\omega L_M \parallel \frac{Z_2 + \left(-j\frac{1}{\omega C_{f2}}\right) \parallel (j\omega L_{f2}) \parallel R_E}{n^2}}{j\omega L_M \parallel \frac{Z_2 + \left(-j\frac{1}{\omega C_{f2}}\right) \parallel R_E \parallel (j\omega L_{f2})}{n^2} + Z_1} \tag{3}$$

$$V_{ab} = nV_{LM} \frac{\left(-j\frac{1}{\omega C_{f2}}\right) \parallel R_E \parallel (j\omega L_{f2})}{Z_2 + \left(-j\frac{1}{\omega C_{f2}}\right) \parallel R_E \parallel (j\omega L_{f2})} \tag{4}$$

where $R_E = \left(\frac{8}{\pi^2}\right)R_L =$ equivalent ac load resistance across the high frequency rectifier side, $Z_1 = j\left(\omega L_{I1} - \frac{1}{\omega C_1}\right)$ and $Z_2 = j\left(\omega L_{I2} - \frac{1}{\omega C_2}\right)$.

By the aid of Fourier analysis, the fundamental component of V_{AB} can be depicted as

$$V_{AB} = \frac{4V_i}{\pi} \tag{5}$$

Due to L_{f2} , majority portion of higher-order harmonics those are tending to inject into the rectifier, can be eliminated. In later, experimental results of LC-LC² compensated resonant converter will compare the efficiency with the results of S-SP compensated resonant converter. Furthermore, V_{ab} can be regarded as a sine wave. Therefore, the simplified voltage across the battery can be written as,

$$V_0 = \frac{1}{\pi} \int_0^\pi V_{ab}(\sin \omega t) d\omega t = \frac{2}{\pi} V_{ab} \tag{6}$$

From Equations (3)–(6), voltage gain of the LC-LC² compensated resonant converter can be represented as,

$$G_V(\omega) = \frac{V_0}{V_i} = \left| \frac{2V_{ab}}{\pi V_{AB}} \right| = \frac{8}{\pi^2} \left| \frac{V_{ab}}{V_{AB}} \right| = \frac{8}{\pi^2} \left| \frac{V_{ab}}{V_{LM}} \cdot \frac{V_{LM}}{V_{AB}} \right| \tag{7}$$

$$= \frac{8}{\pi^2} \left| \frac{n}{1 + \frac{C_{f2}}{L_M} \left[\frac{(Z_2 + n^2 Z_1) j\omega L_M + Z_1 Z_2}{L_M} - (n^2 L_M + L_{f2}) \left(Z_3 + j\frac{1}{\omega C_{f2}} \right) \left(\frac{Z_1}{\omega^2 L_M L_{f2}^2} - j\frac{Z_1 Z_2}{\omega^3 L_M L_{f2}^2 n^2} + \frac{Z_2}{\omega^2 L_M L_{f2}^2 n^2} + \frac{Z_1}{\omega^2 L_M L_{f2}^2 n^2} \right) + j\omega^3 L_M R_E C_1 C_2 \right]} \right|$$

where $Z_3 = j\left(\omega L_{Mf} - \frac{1}{\omega C_{f2}}\right)$ and

$$L_T = L_{I1} + L_M \tag{8}$$

$$L_R = L_{I2} + n^2 L_M \tag{9}$$

$$\delta = \omega^4 C_1 C_2 \left(n^2 L_M^2 - L_T L_R \right) + \omega^2 \left(L_T C_1 + L_R C_2 \right) - 1 \tag{10}$$

Equation (10) can be expressed as,

$$\delta = \omega^2 C_1 C_2 \left[Z_1 Z_2 + j\omega L_M \left(Z_2 + n^2 Z_1 \right) \right] \tag{11}$$

From (7), it is observed that voltage gain is not dependent of the load when $\delta = 0$.

Using $\delta = 0$, frequencies at load independent voltage gain are:

$$\omega_L = \sqrt{\frac{\omega_T^2 + \omega_R^2 - \sqrt{(\omega_T^2 + \omega_R^2)^2 - 4(1 - k^2)\omega_T^2\omega_R^2}}{2(1 - k^2)}} \tag{12}$$

Under the full compensation, (12) and (13) yields,

$$\omega_L = \frac{1}{\sqrt{L_T C_1 + n^2 L_M C_2}} \tag{22}$$

$$\omega_H = \frac{1}{\sqrt{L_{l1} C_1}} \tag{23}$$

Equation (23) follows the Equation (2). Therefore, constant voltage gain and ZPA of input impedance both can be obtained, under the full compensation ($Z_1 = Z_2 = Z_3 = 0$) condition. This is a desired criterion to get high efficiency and output voltage having good controllability. From (7), the required voltage gain can be obtained as,

$$G_V(\omega_r) = \frac{8n}{\pi^2} \tag{24}$$

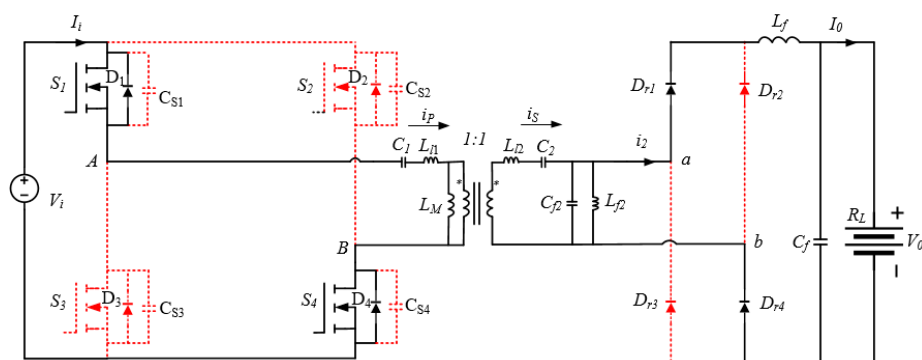
That means with the help of the proposed compensation technique, load independent constant voltage gain is achievable which is desirable for IPT based EV application.

4. LC-LC² Compensated Resonant Converter Using Time Domain Analysis

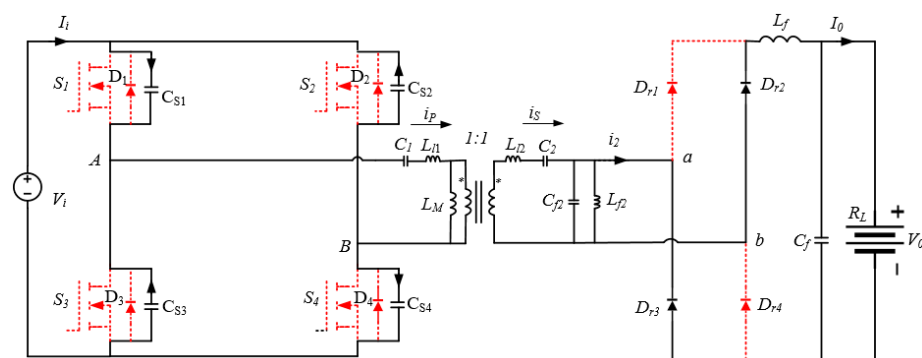
To explain the time domain analysis, the following hypotheses are made:

- (a) All semiconductor switches and diodes are ideal.
- (b) Receiver current, i_s is almost sinusoidal since proposed converter operates near the resonant frequency.

Figure 3a–d depicts the equivalent circuits during different periods of operation of the proposed converter for the operating waveforms shown in Figure 4.

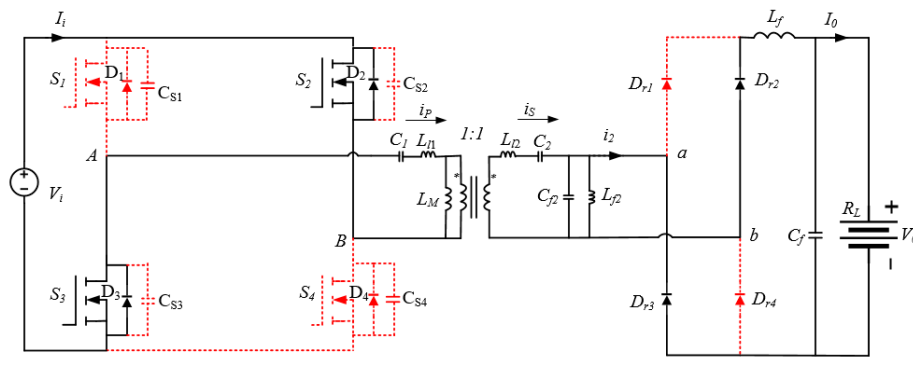


(a) Mode 1 [t_0-t_1]

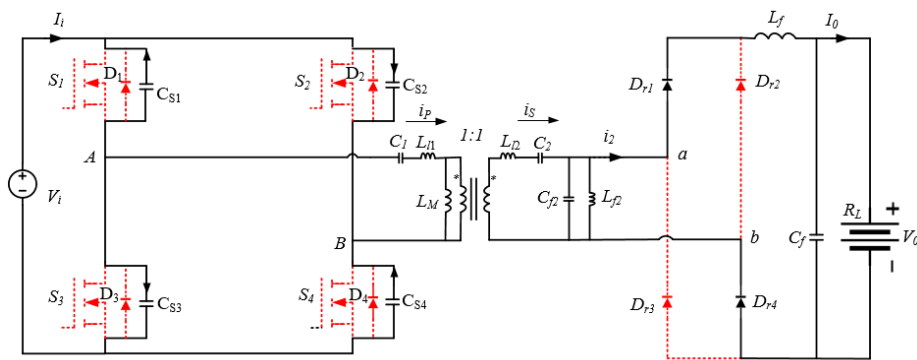


(b) Mode 2 [t_1-t_2]

Figure 3. Cont.



(c) Mode 3 [t2-t3]



(d) Mode 4 [t3-t4]

Figure 3. Equivalent circuit for switching mode (a) Mode 1 [t0-t1]; (b) Mode 2 [t1-t2]; (c) Mode 3 [t2-t3]; (d) Mode 4 [t3-t4].

Considering the time instant t_0 , diagonal switch pair (S_1 and S_4) of the proposed converter is in conduction and another diagonal switch pair (S_2 and S_3) is in off mode. At that time V_{AB} is positively equal to V_i . Firstly, transmitter current i_p passes through the body diodes of S_1 and S_4 , after that S_1 and S_4 start to conduct with the changing of current direction. Consequently, ZVS is obtained.

Throughout this period, current flowing into L_M can be written as,

$$i_{L_M}(t) = \frac{V_i}{L_M} \left(t - \frac{T_S}{4} \right) \tag{25}$$

where T_S is the time period.

Also, receiver current, i_s can be obtained as,

$$i_s(t) = \frac{4n}{\pi} V_i \times \left\{ j \left(\omega C_{f2} - \frac{1}{\omega L_{f2}} \right) + \frac{1}{R_E} \right\} \sin \left(\omega t + \tan^{-1} \left(\omega C_{f2} - \frac{1}{\omega L_{f2}} \right) R_E \right) \tag{26}$$

Therefore, transmitter current, i_p can be calculated as,

$$\begin{aligned} i_p(t) &= i_{L_M}(t) + n i_s(t) \\ &= \frac{V_i}{L_M} \left(t - \frac{T_S}{4} \right) \\ &\quad + n \frac{4n}{\pi} V_i \\ &\quad \times \left\{ j \left(\omega C_{f2} - \frac{1}{\omega L_{f2}} \right) + \frac{1}{R_E} \right\} \sin \left(\omega t + \tan^{-1} \left(\omega C_{f2} - \frac{1}{\omega L_{f2}} \right) R_E \right) \end{aligned} \tag{27}$$

Diagonal switch pair (S_1 and S_4) is in off mode at t_1 . So that i_p charges the C_{S1} and C_{S4} and discharges C_{S2} and C_{S3} . Next, S_1 and S_4 are turned off at zero voltage as C_{S1} and C_{S4} limit the rising voltage rate across the switches. In this case, the direction of i_p can be considered as unchanged because of the short duration of this mode. At time instant t_2 , the voltage across the switches S_2 and S_3 is fully discharged whereas complete charging of the capacitors of S_1 and S_4 occurs from 0 to V_i . Then, to maintain the continuity of i_p , D_2 and D_3 start to conduct. So V_{AB} becomes to $-V_i$.

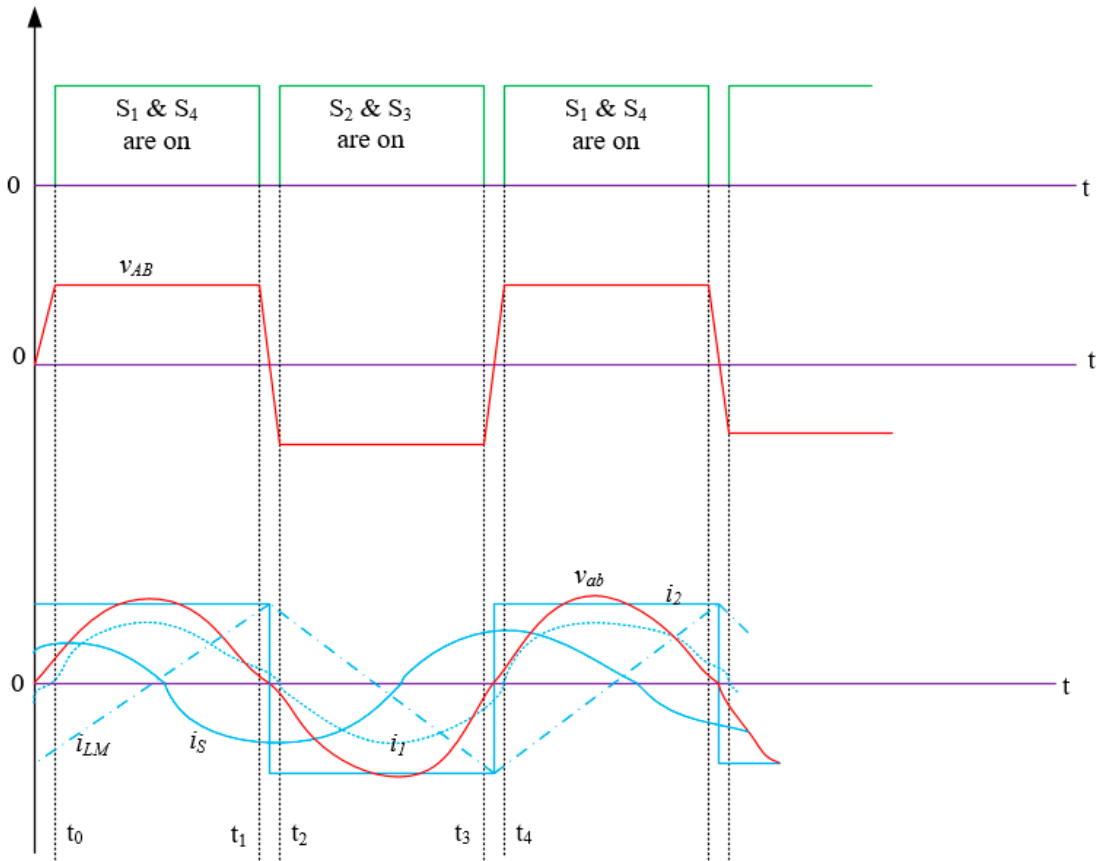


Figure 4. Operating waveforms of the proposed LC-LC2 resonant converter.

After the conduction of D_2 and D_3 , diagonal switch pair (S_2 and S_3) of the proposed converter is in conduction with ZVS. Here, V_{AB} equals to $-V_i$. During this interval, as like to mode 1 current changes its direction. At first, body diodes of S_2 and S_3 conduct, after that S_2 and S_3 start to conduct with the changing of current direction. Throughout this period, current flowing into L_M can be written as,

$$i_{L_M}(t) = \frac{V_i}{L_M} \left(-t + \frac{3T_S}{4} \right) \tag{28}$$

Using (26), transmitter current, i_p can be calculated as,

$$i_p(t) = \frac{V_i}{L_M} \left(-t + \frac{3T_S}{4} \right) + n \frac{4n}{\pi} V_i \times \left\{ j \left(\omega C_{f2} - \frac{1}{\omega L_{f2}} \right) + \frac{1}{R_E} \right\} \sin \left(\omega t + \tan^{-1} \left(\omega C_{f2} - \frac{1}{\omega L_{f2}} \right) R_E \right) \tag{29}$$

Diagonal switch pair (S_2 and S_3) is in off mode with ZVS at t_3 . At time instant t_4 , the voltage across the switches S_1 and S_4 is fully discharged whereas complete charging of the capacitors of S_2 and S_3 occurs from 0 to V_i . Then, to maintain the continuity of i_p , D_1 and D_4 start to conduct. Therefore, ZVS turn on condition occurs for S_1 and S_4 . So, V_{AB} becomes to $+V_i$.

5. Analysis and Experimental Results

The specifications for 500 W LC-LC² compensated resonant converter are as follows: $V_{in} = 211$ V, $V_0 = 171$ V, $P_0 = 500$ W, an air gap of 140 mm. The loosely coupled transformer with a rectangular shape having I shape ferrite core is used in this resonant converter. Although voltage gain is independent of the mutual inductance, capacitors are designed in case of maximum coupling air gap to make resonance with the corresponding inductances. Therefore, at resonant frequency ZVS can be obtained with the specific frequency control. Detailed specifications of the proposed resonant converter with a constant resonant frequency are shown in Table 1.

Table 1. Design specifications of the LC-LC² converter.

Design Specifications	Value
Resonant frequency	$f = 80$ kHz
Parameters of IPT transformer	$n = 1, L_{l1} = 82.95$ μ H, $L_{l2} = 82.05$ μ H, $L_M = 25.25$ μ H–13.1 μ H, $k = 0.234$ –0.140
Compensating inductor	$L_{f2} = 20$ μ H
Resonant capacitors	$C_1 = 47.71$ nF, $C_2 = 48.24$ nF, $C_{f2} = 354.65$ nF
Load resistance	$R_L = 33$ –200 Ω
Filter parameters	$L_f = 1000$ μ H and $C_f = 500$ nF
Load power	$P_L = 500$ W
Air gap	$H = 140$ –180 mm

Figure 5 shows that measured phase angle of the input impedance for an air gap of 140 mm with the specifications listed in Table 1. In accordance with the Figure 5, it is observed that load independent input impedance with ZPA is achieved when the proposed converter is totally compensated.

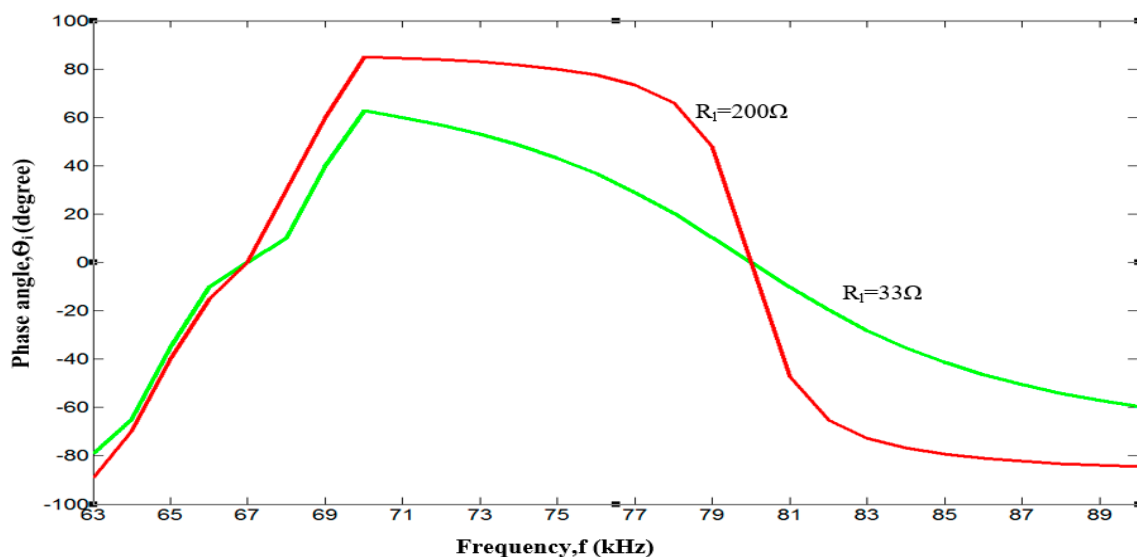


Figure 5. Measured input phase angle of the 500 W LC-LC² compensated resonant converter.

The calculated voltage gain corresponding to the frequency is shown in Figure 6. From Figure 6, load independent voltage gain is found at 80 kHz which follows the Equation (23) as well as Equation (2). Comparing Figures 5 and 6; voltage gain having load independence and input impedance with ZPA, both can be obtained at the frequency of ω_H . The load-regulation curve of the proposed LC-LC² converter from laboratory results is shown in Figure 7.

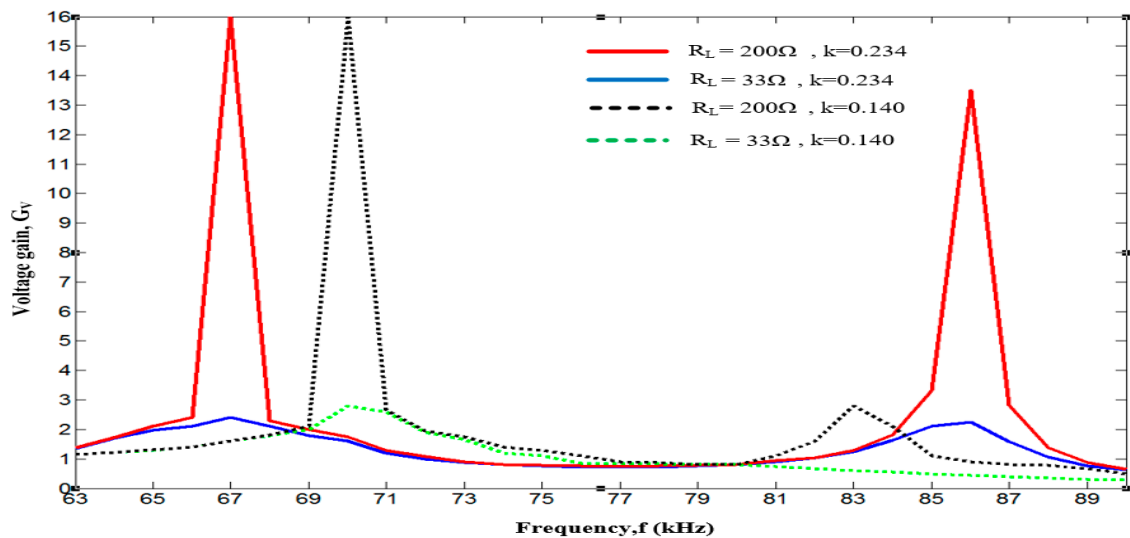


Figure 6. Measured voltage gain of the 500 W LC-LC2 compensated resonant converter.

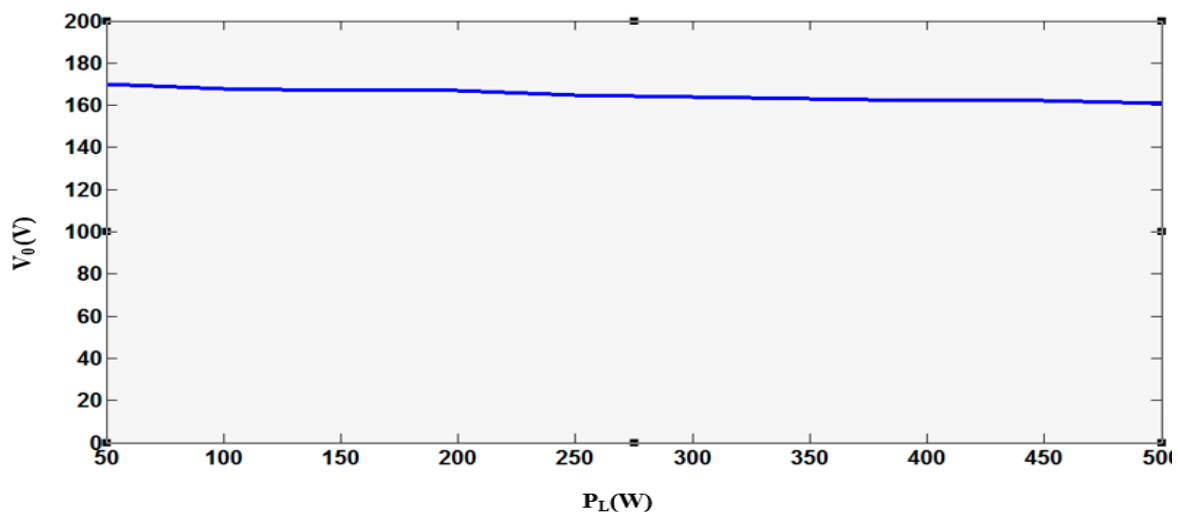


Figure 7. Measured load regulation of the 500 W LC-LC2 compensated resonant converter.

The experimental efficiency from dc source to the battery is calculated for proposed mutual inductance as well as mutual inductance (13.1 μH) for different air gap of 180 mm.

To compare the coupling tolerance of the proposed converter with S-SP compensated resonant converter, the specifications for 500 W S-SP compensated converter are: $V_{in} = 211\text{ V}$, $V_0 = 171\text{ V}$, $P_0 = 500\text{ W}$, $C_1 = 47.71\text{ nF}$, $C_2 = 48.24\text{ nF}$, $C_{f2} = 156.75\text{ nF}$, an air gap of 140 mm, $R_L = 33\text{--}200\ \Omega$. In case of S-SP compensated resonant converter, C_{f2} compensates the mutual inductance, L_M . On the other hand, equivalent inductance $L_{Mf} = n^2 L_M \parallel L_{f2}$ is compensated by C_{f2} in case of the proposed converter.

Comparing Figures 8 and 9, when the mutual inductance is about 13.1 μH , efficiency is much affected in case of S-SP resonant converter. Because efficiency of the S-SP compensated resonant converter directly related to the mutual inductance whereas efficiency of the LC-LC² compensated resonant converter related to the equivalent inductance, $L_{Mf} = n^2 L_M \parallel L_{f2}$. Therefore, LC-LC² compensated resonant converter provides better efficiency than S-SP compensated resonant converter in case of variant air gap condition by which mutual inductance changes. Based on this, it is clear that due to the parallel effect of magnetizing inductance and the additional inductance of the secondary side, phase angle of the input impedance is closely maintained to zero. That's why efficiency is not so much affected by the air gap variation. Also higher order harmonics of i_2 from i_s are limited. Although the proposed compensation technique is built for 140–180 mm air gap variation, the laboratory setup for 140 mm air gap variation is shown in Figure 10.

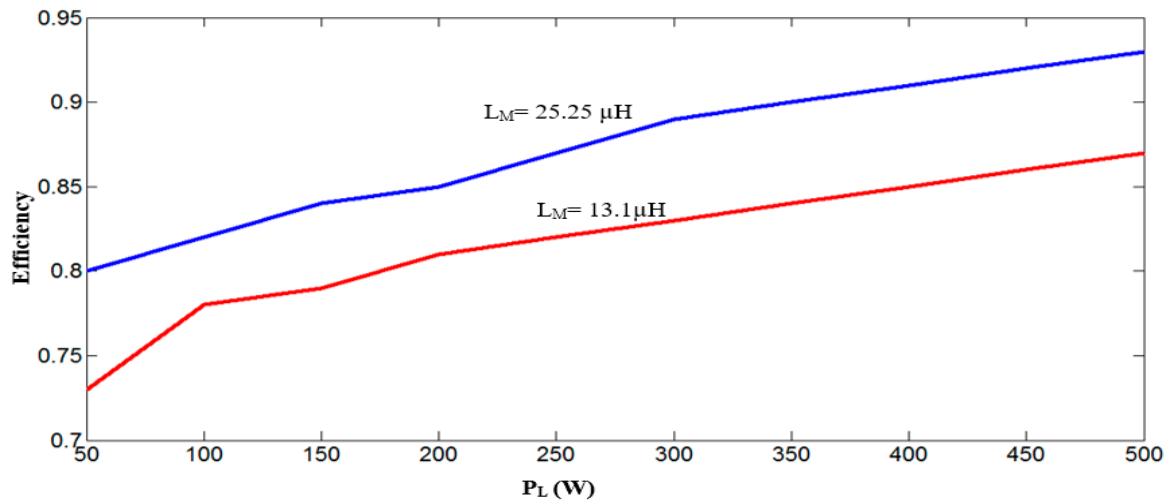


Figure 8. The efficiency of the 500 W LC-LC2 compensated resonant converter.

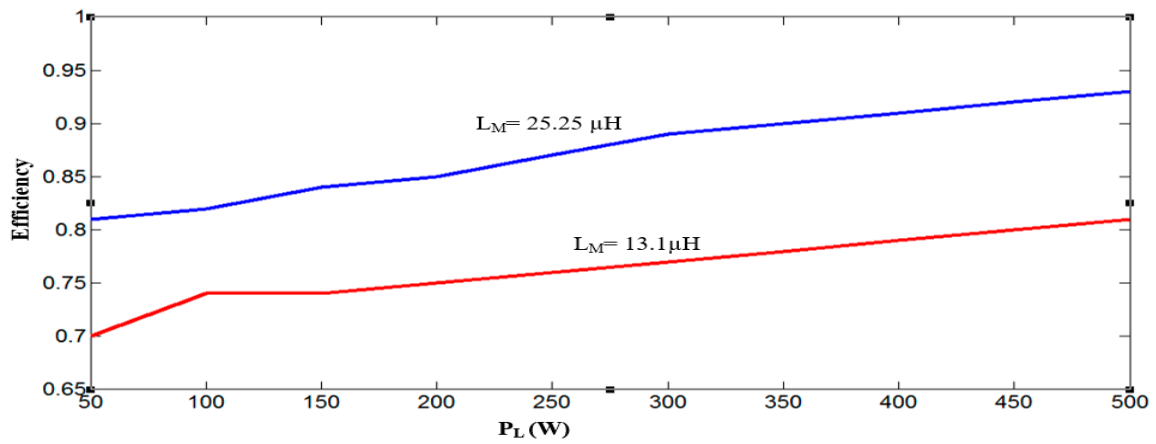


Figure 9. The efficiency of the 500 W S-SP compensated resonant converter.

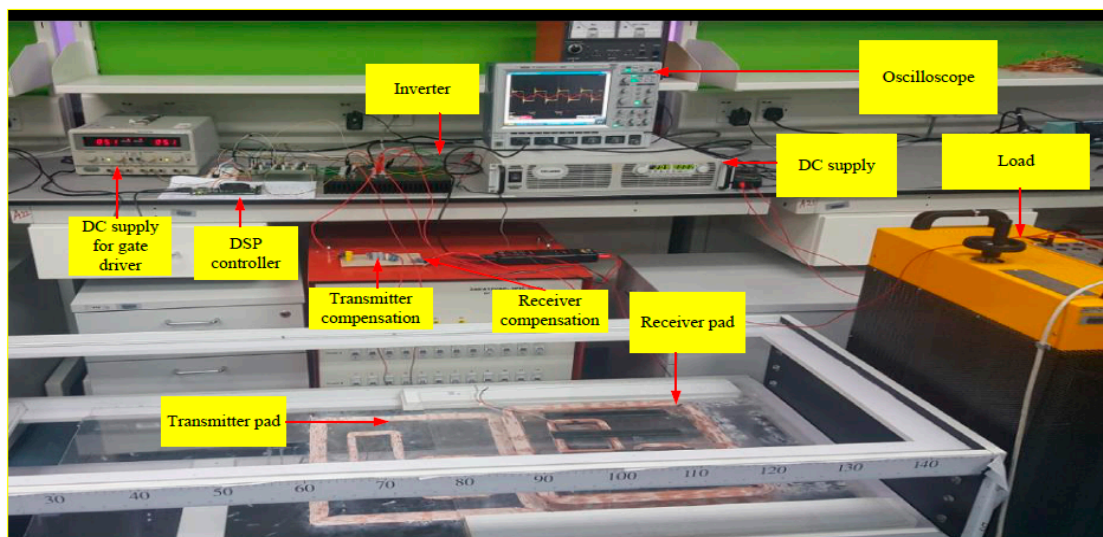


Figure 10. Laboratory results of the proposed LC-LC2 compensated resonant converter.

At the defined air gap, the current i_1 is in phase with the high frequency inverter output voltage V_{AB} . ZVS condition is also observed in case of experimental result which is also shown in Figure 11. In this case, V_{DS} and I_{DS} are the switch voltage and current of the high frequency inverter; V_{GS} is the gate signal.

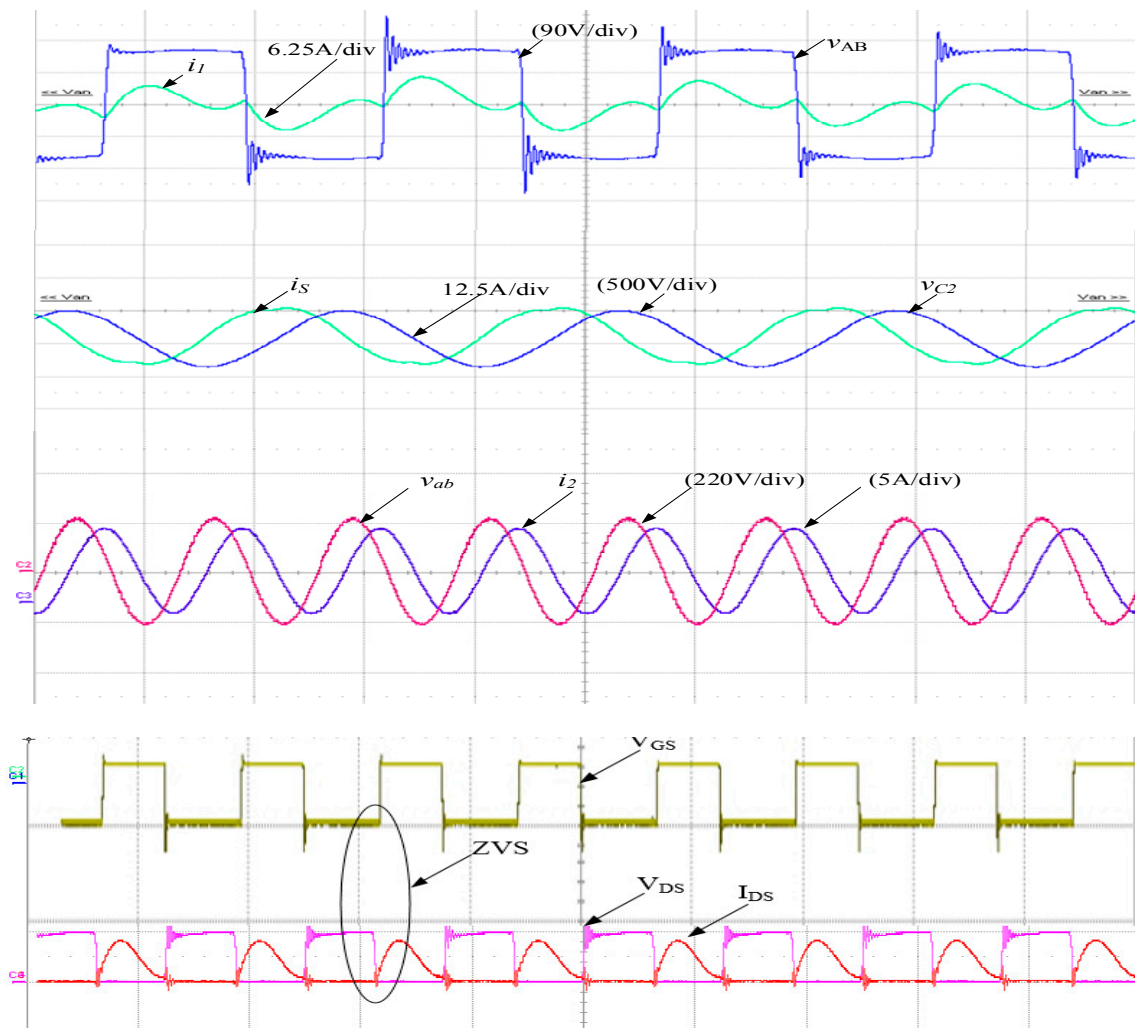


Figure 11. Laboratory results of the proposed LC-LC² compensated resonant converter.

In case of higher-order harmonics injection to the rectifier side, LC-LC² is better than the S-SP compensation technique because of the effect of equivalent inductance L_{Mf} . Comparison between S-SP compensation and LC-LC² compensation is shown in Table 2.

Table 2. Comparison of LC-LC² compensation with S-SP² compensation.

Compensation Networks	Evaluation Criteria				
	Maximum Efficiency	Power Rating	Air Gap	Efficiency Variation	Higher-Order Harmonics
S-SP [18]	93%	1500 W	200 mm	Affected by the mutual inductance changes	Injected to the rectifier side
LC-LC ²	93%	500 W	140 mm	Less affected by the mutual inductance changes	Not injected to the rectifier side

Though above comparison table is for different power rating, efficiency variation by mutual inductance changes and injection of higher order harmonics are the main parameters to evaluate the proposed network. Efficiency variation is not so much affected by the mutual inductance changes in case of proposed compensation based resonant converter in comparison to the S-SP compensation based resonant converter, shown in Figures 8 and 9. Because of an additional receiving side inductor, proposed compensation technique cannot inject higher order harmonics to the rectifier side.

6. Conclusions

The proposed LC-LC² compensated resonant converter provides the input impedance with ZPA and voltage gain having load independent characteristics at a common resonant frequency. Using a common resonant frequency, experimental results of the proposed LC-LC² compensated resonant converter are obtained. Laboratory results represent the efficacy of the proposed compensation method with a maximum efficiency of 93%. In IPT based EV charging application, efficiency is directly related to the air gap variation. Efficiency-comparison between LC-LC² and S-SP compensated resonant converter depicts that efficiency of the LC-LC² compensated resonant converter is not much sensitive to the air gap variation than the S-SP compensated resonant converter. Due to the less sensitivity of the air gap variation, proposed compensation technique is very much effective in the IPT based EV charging application.

Author Contributions: Theoretical observation, simulation, experimental tests, and preparing the article are contributed by M.M.A.; S.M. has the contribution in experimental tests and preparation of the article, H.B. has the contribution in theoretical approaches and preparing the article and M.J.H.R. has contributed to the theoretical explanation and preparing the article.

Funding: The authors would like to acknowledge the financial support received from the University of Malaya, Malaysia, through Frontier Research Grant No. FG007-17AFR and Innovative Technology Grant No. RP043B-17AET.

Conflicts of Interest: There is no conflict of interest in author's declaration.

References

- Cong, Z.; Jih-Sheng, L.; Rui, C.; Faraci, W.E.; Zahid, Z.U.; Bin, G.; Anderson, D. High-Efficiency Contactless Power Transfer System for Electric Vehicle Battery Charging Application. *IEEE J. Emerg. Sel. Top. Power Electron.* **2015**, *3*, 65–74. [[CrossRef](#)]
- Zhong, C.; Wuwei, J.; Xuiliang, H.; Linlin, T.; Chen, C.; Wang, W. A Promoted Design for Primary Coil in Roadway-Powered System. *IEEE Trans. Magn.* **2015**, *51*, 1–4. [[CrossRef](#)]
- Sallan, J.; Villa, J.L.; Llombart, A.; Sanz, J.F. Optimal Design of ICPT Systems Applied to Electric Vehicle Battery Charge. *IEEE Trans. Ind. Electron.* **2009**, *56*, 2140–2149. [[CrossRef](#)]
- Lu, F.; Zhang, H.; Hofmann, H.; Mi, C. A Dynamic Charging System with Reduced Output Power Pulsation for Electric Vehicles. *IEEE Trans. Ind. Electron.* **2016**, *63*, 6580–6589. [[CrossRef](#)]
- Kainan, C.; Zhengming, Z. Analysis of the Double-Layer Printed Spiral Coil for Wireless Power Transfer. *IEEE J. Emerg. Sel. Top. Power Electron.* **2013**, *1*, 114–121.
- Raju, S.; Rongxiang, W.; Mansun, C.; Yue, C.P. Modeling of Mutual Coupling Between Planar Inductors in Wireless Power Applications. *IEEE Trans. Power Electron.* **2014**, *29*, 481–490. [[CrossRef](#)]
- Chen, Q.; Wong, S.C.; Tse, C.K.; Ruan, X. Analysis, Design, and Control of a Transcutaneous Power Regulator for Artificial Hearts. *IEEE Trans. Biomed. Circuits Syst.* **2009**, *3*, 23–31. [[CrossRef](#)] [[PubMed](#)]
- Klontz, K.W.; Divan, D.M.; Novotny, D.W.; Lorenz, R.D. Contactless power delivery system for mining applications. In Proceedings of the Conference Record of the 1991 IEEE Industry Applications Society Annual Meeting, Dearborn, MI, USA, 28 September–4 October 1991; pp. 1263–1269.
- Budhia, M.; Boys, J.T.; Covic, G.A.; Chang-Yu, H. Development of a Single-Sided Flux Magnetic Coupler for Electric Vehicle IPT Charging Systems. *IEEE Trans. Ind. Electron.* **2013**, *60*, 318–328. [[CrossRef](#)]
- Wei, Z.; Siu-Chung, W.; Tse, C.K.; Qianhong, C. Design for Efficiency Optimization and Voltage Controllability of Series-Series Compensated Inductive Power Transfer Systems. *IEEE Trans. Power Electron.* **2014**, *29*, 191–200.
- Huh, J.; Lee, S.W.; Lee, W.Y.; Cho, G.H.; Rim, C.T. Narrow-Width Inductive Power Transfer System for Online Electrical Vehicles. *IEEE Trans. Power Electron.* **2011**, *26*, 3666–3679. [[CrossRef](#)]
- Chwei-Sen, W.; Covic, G.A.; Stielau, O.H. Power transfer capability and bifurcation phenomena of loosely coupled inductive power transfer systems. *IEEE Trans. Ind. Electron.* **2004**, *51*, 148–157.
- Raabe, S.; Covic, G.A. Practical Design Considerations for Contactless Power Transfer Quadrature Pick-Ups. *IEEE Trans. Ind. Electron.* **2013**, *60*, 400–409. [[CrossRef](#)]

14. Keeling, N.A.; Covic, G.A.; Boys, J.T. A Unity-Power-Factor IPT Pickup for High-Power Applications. *IEEE Trans. Ind. Electron.* **2010**, *57*, 744–751. [[CrossRef](#)]
15. Wu, H.H.; Gilchrist, A.; Sealy, K.D.; Bronson, D. A High Efficiency 5 kW Inductive Charger for EVs Using Dual Side Control. *IEEE Trans. Ind. Inform.* **2012**, *8*, 585–595. [[CrossRef](#)]
16. Wei, Z.; Siu-Chung, W.; Tse, C.K.; Qianhong, C. Analysis and Comparison of Secondary Series- and Parallel-Compensated Inductive Power Transfer Systems Operating for Optimal Efficiency and Load-Independent Voltage-Transfer Ratio. *IEEE Trans. Power Electron.* **2014**, *29*, 2979–2990.
17. Villa, J.L.; Sallan, J.; Sanz, J.F.; Llombart, A. High-Misalignment Tolerant Compensation Topology For ICPT Systems. *IEEE Trans. Ind. Electron.* **2012**, *59*, 945–951. [[CrossRef](#)]
18. Hou, J.; Chen, Q.; Yan, K.; Ren, X.; Wong, S.C.; Tse, C.K. Analysis and control of S/SP compensation contactless resonant converter with constant voltage gain. In Proceedings of the IEEE Energy Conversion Congress and Exposition, Denver, CO, USA, 15–19 September 2013; pp. 2552–2558.
19. Budhia, M.; Covic, G.A.; Boys, J.T.; Chang-Yu, H. Development and evaluation of single sided flux couplers for contactless electric vehicle charging. In Proceedings of the IEEE Energy Conversion Congress and Exposition (ECCE), Phoenix, AZ, USA, 17–22 September 2011; pp. 614–621.
20. Ahmed, K.; Aamir, M.; Uddin, M.K.; Mekhilef, S. A new coil design for enhancement in misalignment tolerance of Wireless Charging System. In Proceedings of the IEEE Student Conference on Research and Development (SCORED), Kuala Lumpur, Malaysia, 13–14 December 2015; pp. 215–219.
21. Boys, J.T.; Covic, G.A.; Green, A.W. Stability and control of inductively coupled power transfer systems. *IEEE Proc.-Electr. Power Appl.* **2000**, *147*, 37–43. [[CrossRef](#)]
22. Chwei-Sen, W.; Stielau, O.H.; Covic, G.A. Design considerations for a contactless electric vehicle battery charger. *IEEE Trans. Ind. Electron.* **2005**, *52*, 1308–1314.
23. Zhu, Q.; Wang, L.; Guo, Y.; Liao, C.; Li, F. Applying LCC Compensation Network to Dynamic Wireless EV Charging System. *IEEE Trans. Ind. Electron.* **2016**, *63*, 6557–6567. [[CrossRef](#)]
24. Weihan, L.; Han, Z.; Tianze, K.; Mi, C. Inter-operability considerations of the double-sided LCC compensated wireless charger for electric vehicle and plug-in hybrid electric vehicle applications. In Proceedings of the IEEE PELS Workshop on Emerging Technologies: Wireless Power (2015 WoW), Daejeon, Korea, 5–6 June 2015; pp. 1–6.
25. Xiaoyong, R.; Qianhong, C.; Lingling, C.; Xinbo, R.; Siu-Chung, W.; Tse, C.K. Characterization and control of self-oscillating contactless resonant converter with fixed voltage gain. In Proceedings of the 7th International Power Electronics and Motion Control Conference, Harbin, China, 2–5 June 2012; pp. 1822–1827.
26. Hasanzadeh, S.; Vaez-Zadeh, S. Enhancement of overall coupling coefficient and efficiency of contactless energy transmission systems. In Proceedings of the 2nd Power Electronics, Drive Systems and Technologies Conference, Tehran, Iran, 16–17 February 2011; pp. 638–643.
27. Li, W.; Zhao, H.; Li, S.; Deng, J.; Kan, T.; Mi, C.C. Integrated LCC Compensation Topology for Wireless Charger in Electric and Plug-in Electric Vehicles. *IEEE Trans. Ind. Electron.* **2015**, *62*, 4215–4225. [[CrossRef](#)]
28. Huang, C.Y.; Boys, J.T.; Covic, G.A. LCL Pickup Circulating Current Controller for Inductive Power Transfer Systems. *IEEE Trans. Power Electron.* **2013**, *28*, 2081–2093. [[CrossRef](#)]
29. Amjad, M.; Salam, Z.; Facta, M.; Mekhilef, S. Analysis and Implementation of Transformerless LCL Resonant Power Supply for Ozone Generation. *IEEE Trans. Power Electron.* **2013**, *28*, 650–660. [[CrossRef](#)]

